Journal of the European Ceramic Society 21 (2001) 1143–1150

www.elsevier.com/locate/jeurceramsoc

AC impedance study of Ni, Fe, Cu, Mn doped ceria stabilized zirconia ceramics

C.R. Foschini [a,*], D.P.F. Souza [b], P.I. Paulin Filho [b], J.A. Varela [a]

[a] *Instituto de Química, Universidade Estadual Paulista, UNESP, Araraquara, SP, 14801-970, Brazil*
[b] *Dpt. de Eng. de Materiais, Univ. Federal de São de Carlos, UFSCar, S. Carlos, SP, 13565-905, Brazil*

Received 6 July 2000; received in revised form 30 October 2000; accepted 21 November 2000

Abstract

Doped zirconia has been used in electronic applications in the cubic crystalline phase. Ceria-stabilized tetragonal zirconia presents high toughness and can also be applied as solid electrolytes. The tetragonal phase of zirconia can be stabilized at room temperature with ceria in a broad range of composition. However, CeO_2–ZrO_2 has low sinterability, so it is important to investigate the effect of sintering dopants. In this study the effect of iron, copper, manganese and nickel was investigated. The dopants such as iron and copper lowered the sintering temperature from 1600°C down to 1450°C, with a percentage of tetragonal phase retained at room temperature higher than 98% and also with an increase of the electrical conductivity. The electrical conductivity was measured using impedance spectroscopy. The grain boundary contribution was determined and the activation energy associated with the ionic conduction was 1.04 eV. The dopants can also promote a grain boundary cleanliness verified by blocking effect measurement.

Keywords: CeO_2-ZrO_2; Electrical properties; Impedance spectroscopy; Sintering; ZrO_2

1. Introduction

The zirconium oxide, known as zirconia, has three polymorphic phases: monoclinic ($T < 1170$°C), tetragonal ($1170 < T < 2370$°C) and cubic ($T > 2370$°C). The preparation of tetragonal zirconia can be made by either adding 3 mol% Y_2O_3[1] or 12 mol% CeO_2.[2] The ceria-zirconia system is being developed as an alternative to the yttria-zirconia system because of its better performance in a moist environment, [3] good mechanical properties,[4] lower price and wider range of solubility.[5] Unfortunately, cerium ions are less effective than yttrium ones in stabilizing the tetragonal phase of zirconia, and generates a low sinterability system.[6] In the case of yttria-zirconia, the tetragonal phase is retained due to the presence of oxygen vacancies, which account for the charge neutrality. In the case of ceria-zirconia, the Ce ions also substitute for Zr^{4+} ions, but they can have two valence states: Ce^{3+} and Ce^{4+}.[7]

The effect of sintering aids such as copper and manganese ions on the sintering behavior of ceria-stabilized zirconia was investigated by Mashio et al.[8] The authors verified that MnO_2 as well as CuO were very effective in improving the tetragonal phase content retained at room temperature.

In this work we have studied the effect of the sintering aids such as nickel, iron, copper and manganese on the electrical properties of the ceria-zirconia system. With the use of these sintering aids for Ce-doped tetragonal zirconia polycrystals (Ce-TZP), we were able to produce a dense ceramic material, with an uniform microstructure, stabilized more than 98% in the tetragonal phase and sintered at temperatures up to 150°C lower than that for undoped CeO_2–ZrO_2 system.

2. Experimental

Commercial zirconium oxide (>99.9% in purity) and cerium oxide (>99.0% in purity) were mixed using zirconia balls in isopropyl alcohol medium to produce powders with the following composition 88 mol% ZrO_2–12 mol% CeO_2. In order to study the influence of additives, the dried ZrO_2–12%CeO_2 powder was divided into five batches: (1) as prepared powder labeled ZrCe; (2)

* Corresponding author. Tel.: +55-16-2016641.
E-mail address: foschini@iq.unesp.br (C.R. Foschini).

0955-2219/01/$ - see front matter
PII: S0955-2219(00)00339-3

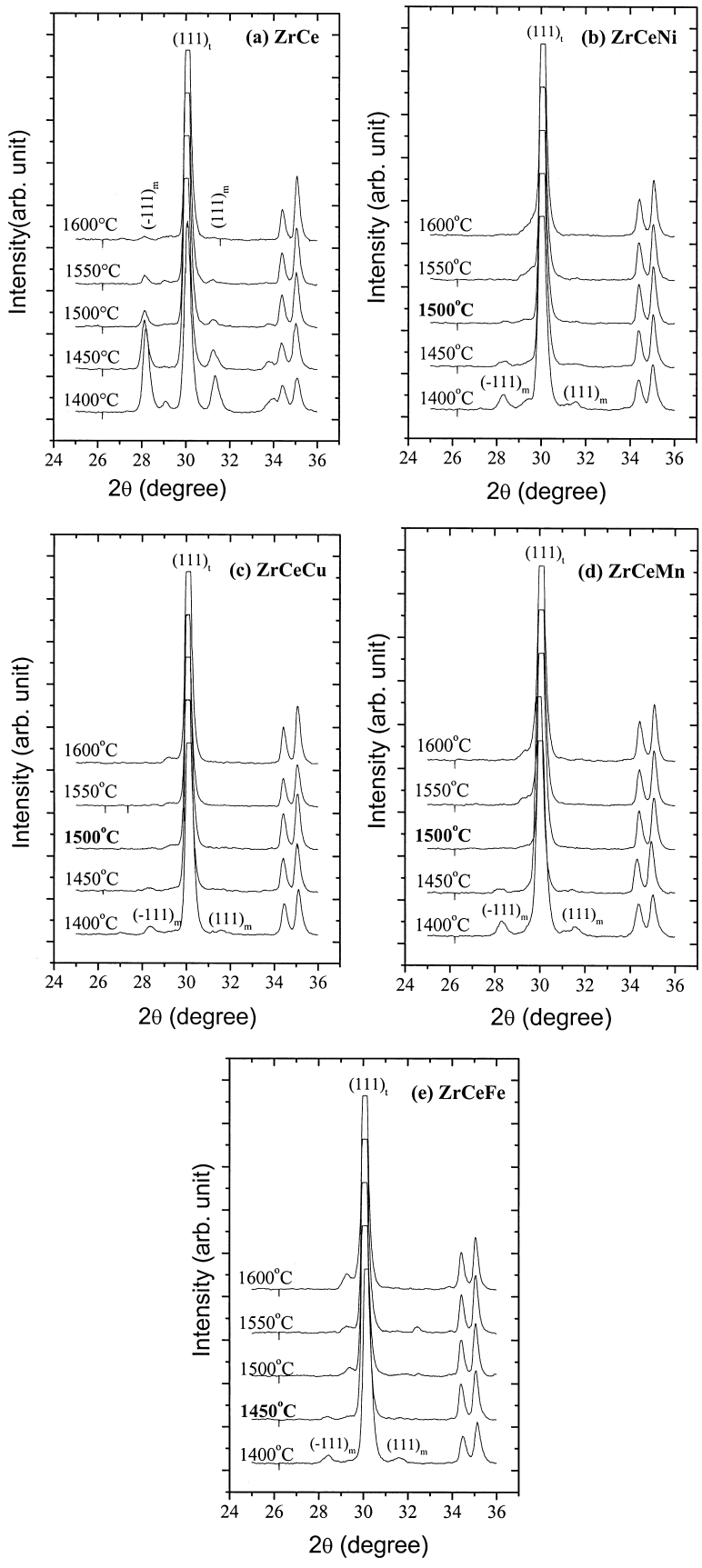

Fig. 1. X-ray diffraction patterns of ZrO_2–12 mol% CeO_2 with different dopants sintered in a temperature range of 1400–1600°C.

ZrCe + 0.3 mol% NiO, labeled ZrCeNi; (3) ZrCe + 0.3 mol% Fe_2O_3, labeled ZrCeFe; (4) ZrCe + 0.3 mol% CuO, labeled ZrCeCu; (5) ZrCe + 0.3 mol% MnO, labeled ZrCeMn. Nickel and iron nitrates, copper and manganese acetates (Riedel del Haën) were added and ball milled in plastic jars with zirconia balls for 30 h with an organic defloculant. Powders were calcinated at 500°C to eliminate volatiles, ball milled in isopropyl alcohol with the addition of 1 wt.% of polyvinyl butyral (PVB), dried at room temperature, and sieved through an 80 mesh nylon sieve. Pellets of 12 mm diameter were isostatically pressed at 270 MPa and sintered in the range of 1400–1600°C for 1 h in air.

The apparent densities of the sintered pellets were measured using Archimedes' method with distilled water. XRD (Siemens D-5000) was used to analyze the sintered pellets for phase identification. SEM (Carl Zeiss DSM 940A) was used to study the microstructure. Samples were ground with successive grades of SiC papers; polished with 15, 6, 3 and 1 μm grits of diamond paste and thermal etched at 50°C below the sintering temperature during 10 min. The dilatometric study was performed in a dilatometer (Netzsch 402E) up to 1500°C using a constant heating rate of 10°C/min. Electrical measurements were performed on polished pellets with platinum electrodes applied by painting (Demetron 308A). The grain electrical conductivity was measured by impedance spectroscopy technique using the impedance analyzer (HP 4192A LF) in the frequency and temperature range of 5 Hz–13 MHz and 300–700°C respectively, during heating with a hold time of 30 min in each temperature.

3. Results and discussion

Table 1 summarizes the values of sintering temperature, apparent density and percentage of tetragonal phase retained at room temperature after sintering. The sintering temperature was chosen based on the X-ray diffraction. Fig. 1 shows XRD patterns of samples with different compositions sintered at different temperatures. As one can observe, the presence of additives can decrease the stabilization temperature of tetragonal phase up to ~150°C in the case of iron.

The dilatometry data also indicated that the additives promote the ZrCe densification and that copper and iron are the most efficient. From Fig. 2(a), we can observe that the starting temperature of shrinkage was 1220°C for ZrCe sample and 1100°C for compositions with iron and copper. Fig. 2(b) displays the shrinkage rate versus temperature, a dense sample was obtained at 1425°C for the

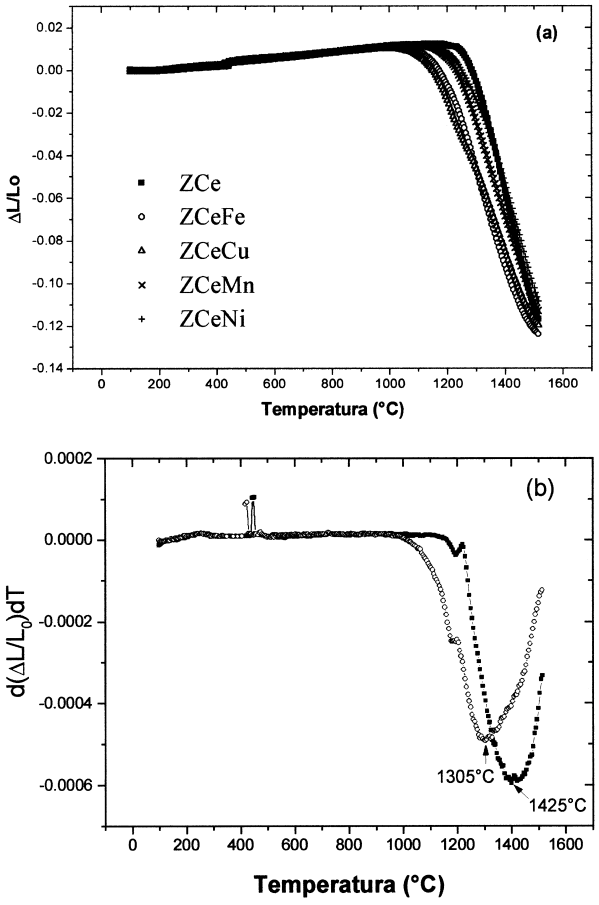

Fig. 2. Dilatometric curves for the different starting powders (a) and (b) the shrinkage rate vs. temperature for ZrCe and ZrCeFe compositions.

Table 1
Sintering temperature, apparent density, percentage of tetragonal phase retained at room temperature and average grain size of CeO_2–ZrO_2 samples undoped and Ni, Fe, Cu and Mn doped

Sample	Temperature (°C)	Apparent density (g/cm³)	Percentage of tetragonal phase (%)[a]	Average grain size (μm)[b]
ZrCe	1600	5.65	99.4	1.22±0.58
ZrCeNi	1500	5.79	99.7	1.27±0.59
ZrCeFe	1450	5.63	98.6	1.19±0.59
ZrCeCu	1500	5.87	100.0	1.21±0.58
ZrCeMn	1500	5.76	99.7	1.18±0.57

[a] Percentage of tetragonal phase content retained at room temperature by the Rietveld method.
[b] Average grain size obtained from Feature Analysis Imix V9 Program, PGT, Princeton Gamma-Tech. 1998.

ZrCe and at 1305°C for ZrCeFe composition. The small expansion at 400°C is related with the loss of binder and the inflection at 1170°C with the phase transition from monoclinic to tetragonal.

Fig. 3(a)–(e) shows microstructures of various specimens. The results of grain size measurements are given in Table 1. The average grain size, measured by a feature analysis program and illustrated in Fig. 4, was similar for

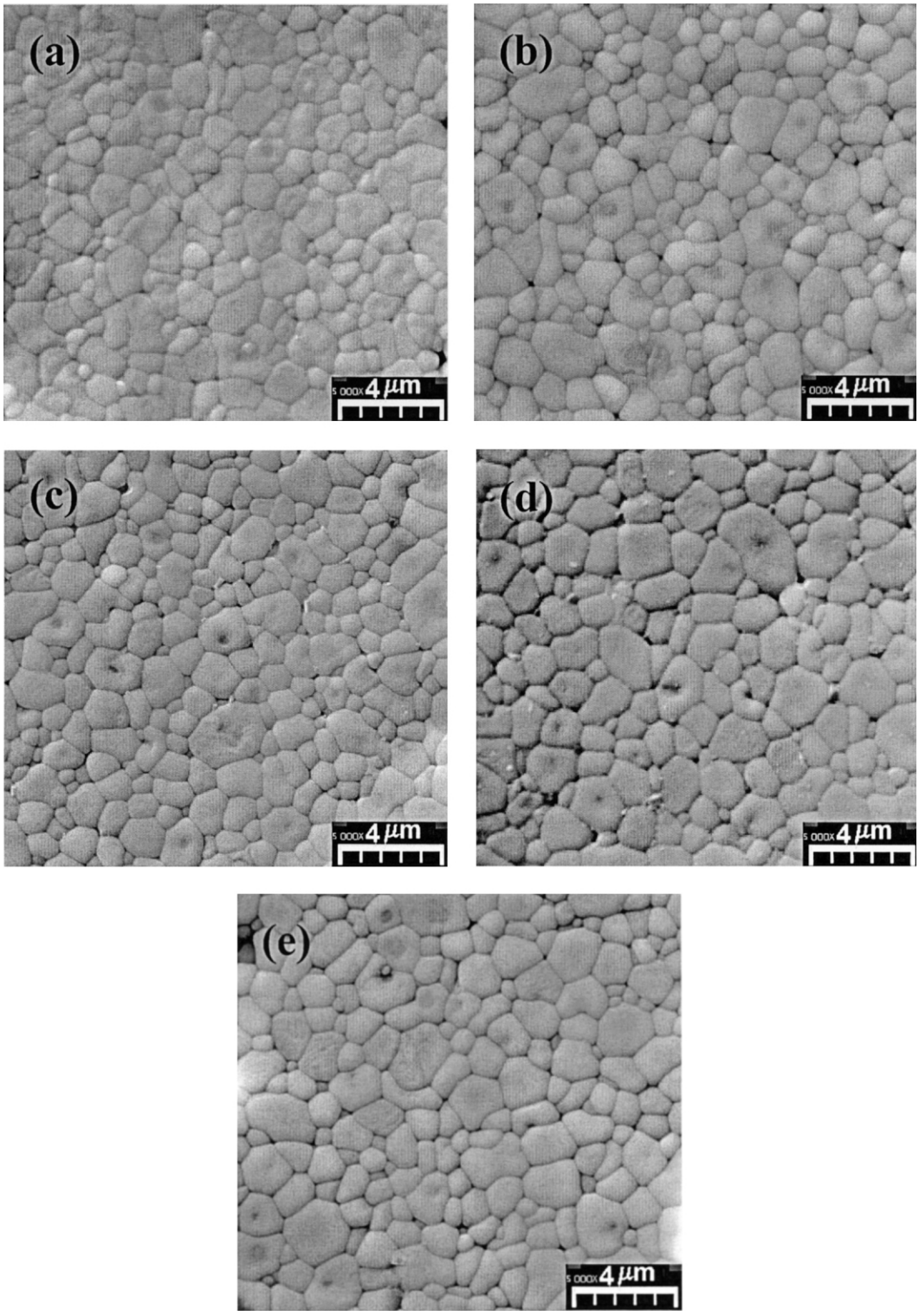

Fig. 3. Scanning electron micrographs of various specimens. (a) ZrCe; (b) ZrCeFe; (c) ZrCeMn; (d) ZrCeCu; (e) ZrCeNi.

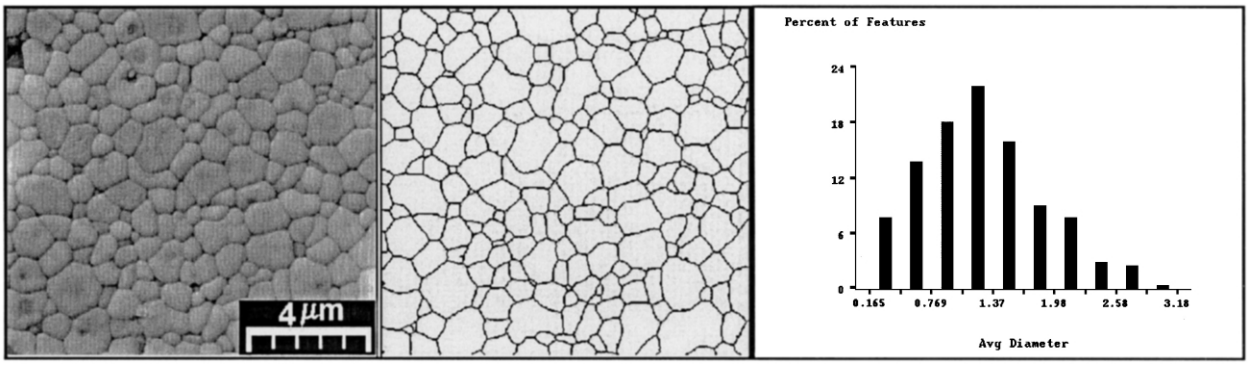

Fig. 4. Average grain size measurement in ZrCeNi sample.

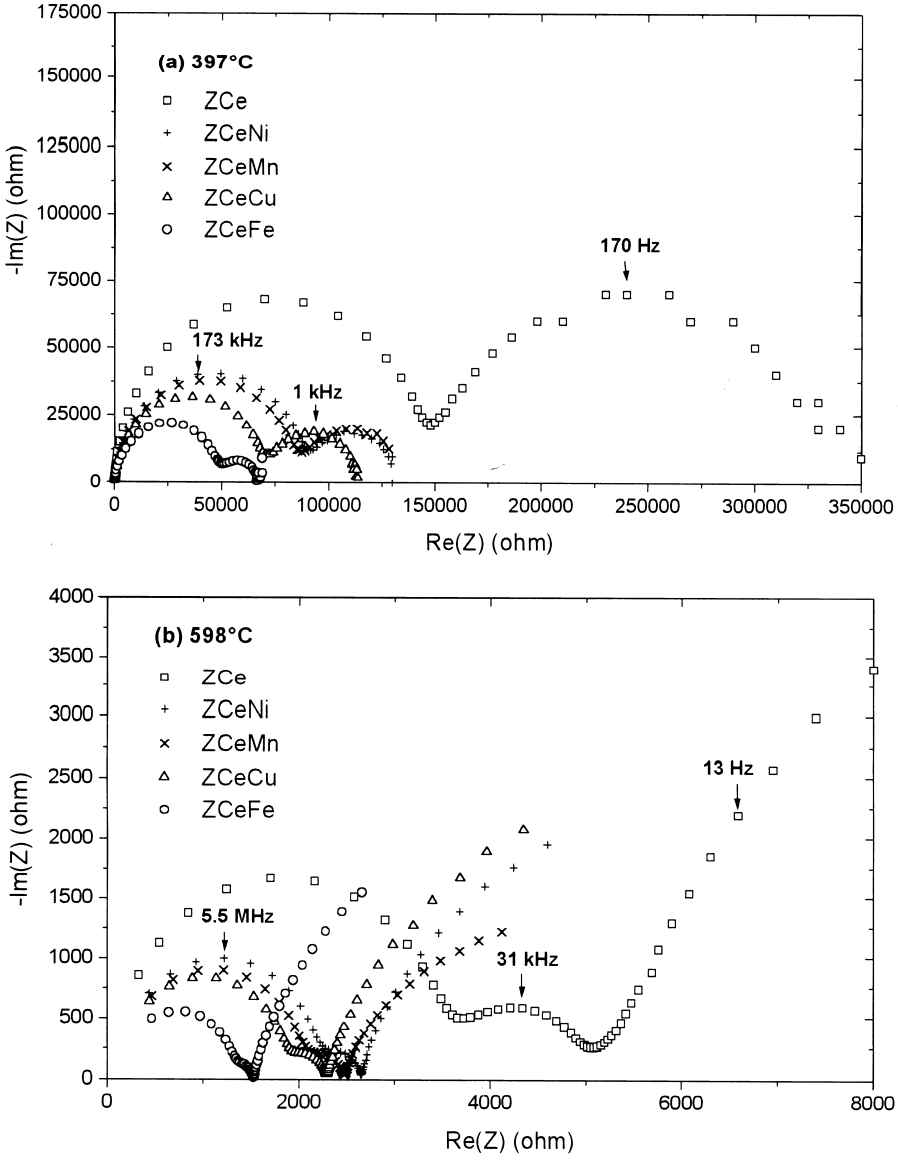

Fig. 5. Impedance plots at (a) 397°C and (b) 598°C.

all specimens examined and was in the range of 1.18–1.27 μm. It was also observed an inhomogeneous grain size distribution and practically no residual porosity.

Fig. 5(a)–(b) shows the impedance diagrams obtained at 397 and 598°C respectively. Measurements were performed in air. Through this technique it was possible to separate the contribution of the grain and the grain boundary resistivities. In Fig. 5(a) and (b), for each specimen, the arc on the left (next to the Y or the imaginary impedance axis) is due to the intragrain resistivity and the arc on the right (next to the intragrain resistivity arc) is due to the intergrain resistivity. The difference of intercepts of each arc on the X or real impedance axis gives resistivity associated with the intra or intergrain process. The arc on the extreme right (just appearing on the low frequency end of the impedance diagrams) is due to the relaxation of the electrode process. It can be observed that the presence of transition metals decreased the sample electrical resistivity of grain and grain boundary when compared with the composition ZrCe. The ZrCeFe composition showed the lowest resistance. This reduction promoted by the iron in the electrical resistance could be associated with the contribution of the electronic conduction due to the presence of Fe^{+3} and Fe^{+2}. However, it can be observed that there is no significant alteration in the impedance spectra for the different compositions. That is, the spectra for all compositions are formed by simple semicircles with their centers on the axis x. It was also observed in the Arrhenius's plots [Fig. 6(a) and (b)] no variation in the slope over the entire temperature range of measurements for the specimens with iron content, neither for intragrain nor for grain boundary conductivities. The activation energy values calculated from the Arrhenius's plots in the temperature range of 350–700°C for intragrain and grain boundary conductivities are given in Table 2. These results are in good agreement with the literature [9] and suggest that the conduction is mainly due to ionic diffusion. At high temperature range, the contribution from the grain boundary resistivity to the total resistivity is expected to be relatively small because the activation energy associated with oxygen-ion migration within the zirconia lattice is much lower than that for the grain boundary resistivity. In this way, the role of the grain boundary or the impurity phases (if present) becomes more critical in the low temperature range. The activation energy in the low temperature range consists of activation energy of defect migration as well as activation energy for dissociation of defect-associates whereas in the high temperature range where most defect-associates dissociate, the activation energy is likely to be mainly due to migration of oxygen-ion vacancies.[10, 11]

Table 2
Activation energy values calculated from the impedance data for grain (E_{ag}) and grain boundary (E_{agb}) conductivity

Composition	E_{ag} (eV)	E_{agb} (eV)
ZrCe	1.03±0.02	1.26±0.03
ZrCeCu	1.01±0.01	1.26±0.02
ZrCeNi	1.03±0.01	1.25±0.02
ZrCeMn	1.04±0.01	1.25±0.04
ZrCeFe	1.04±0.02	1.22±0.03

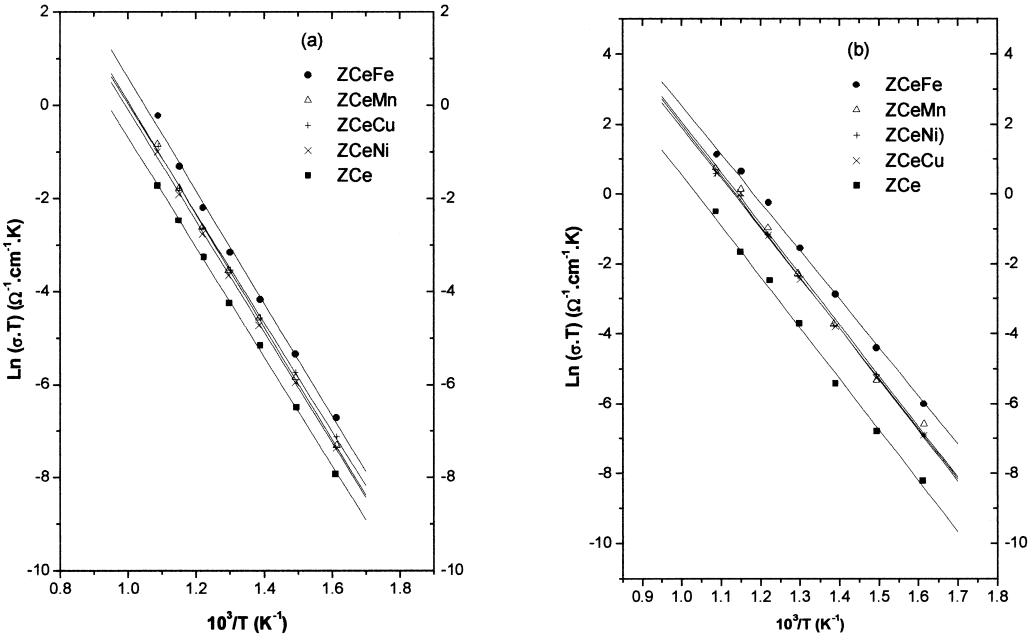

Fig. 6. Arrhenius plots for (a) intragrain and (b) grain boundary conductivities.

Table 3
Blocking factor (α) measured at 400, 500 and 600°C

Composition	$\alpha_{400°C}$	$\alpha_{500°C}$	$\alpha_{600°C}$
ZrCe	0.58	0.37	0.31
ZrCeCu	0.39	0.25	0.14
ZrCeNi	0.31	0.21	0.13
ZrCeMn	0.38	0.22	0.13
ZrCeFe	0.28	0.17	0.12

The influence of the grain boundary conductivity in the total conductiviy can be evaluated through the blocking factor (α_R) [12–15] defined from the impedance diagram parameters by:

$$\alpha_R = R_{gb}/(R_g + R_{gb})$$

where R_g and R_{gb} are grain and grain boundary resistivities respectively. This factor gives the fraction of the electric carriers being blocked at the impermeable internal surfaces, under the measuring conditions, with respect to the total number of electric carriers in the sample. Table 3 shows the blocking factor as a function of temperature for all compositions. The lowest blocking factor was observed in the iron-doped composition for all ranges of temperature. It is well known that during sintering and grain growth, impurities tend to accumulate at grain boundaries, react with each other and undergo phase exchanges with the bulk matrix components.[16–20] Also glassy phases at grain boundaries and triple grain junctions can contain significant amount of yttrium removed from the neighbouring zirconia-yttria grains.[18–20] Many of these glassy phases are molten at the sintering temperature ($\geqslant$1450°C) used in this study and, therefore, are quite mobile. The assumption that the observed blocking effect in stabilized zirconia results directly from the formation of blocked zones, where electric carriers are trapped and do not contribute to the transport of electric current. This effect decreases as the conductivity of the matrix increases . These results suggest that the iron can promote grain boundary cleanliness, i.e. it can be promoting the impurities segregation in the specific places of the microstructure, such as in the triple point. This behaviour is well known in zirconia–yttria compositions, where alumina promotes the silica segregation at the triple point.[21] Further investigation will be carried out using HTEM to clarify the possible liquid phase formation at the grain boundary.

4. Conclusion

Addition of 0.3 mol% of transition metals such as Ni, Fe, Cu and Mn decrease both sintering temperature and stabilization temperature of Ce-stabilized zirconia up to 150°C when compared with the undoped Ce–ZrO_2 system.

The transition metals do not affect the conduction mechanism, as verified through the Arrhenius's plots. Beside the increase in the lattice conductivity, up to three times, the dopants decrease substantially the grain boundary blocking factor, being Fe_2O_3 more effective. This could indicate that the dopants are forming a liquid phase during sintering which can clean the grain boundary by segregation of impurities at triple point.

Acknowledgements

The authors acknowledge the financial support of CNPq, CAPES and FAPESP, agencies from Brazil.

References

1. Ruiz, L. and Readey, M. J., Effect of heat treatment on grain size, phase assemblage, and mechanical properties of 3 mol% Y–TZP. *J. Am. Ceram. Soc.*, 1996, **79**(9), 2331–2340.
2. Wang, J., Zheng, X. H. and Stevens, R., Fabrication and microstructure-mechanical property relationships in Ce–TZPs. *J. Mater. Sci.*, 1992, **27**(19), 5348–5356.
3. Matsumoto, R. L. K., Aging behavior of ce-stabilized tetragonal zirconia polycrystals. *J. Am. Ceram. Soc.*, 1978, **71**(3), C128–129.
4. Sukuma, K. and Shimada, M., Strength, fracture toughness and vickers hardness of CeO_2-stabilized tetragonal ZrO_2 polycrystals (Ce–TZP). *J. Mater. Sci.*, 1985, **20**, 1178–1184.
5. Wang, J., Zheng, X. H. and Stevens, R., Fabrication and microstructure-mechanical property relationships in Ce–TZPs. *J. Mater Sci.*, 1992, **27**, 5348–5356.
6. Zhu, H. Y., CeO_{15}-stabilized tetragonal ZrO_2. *J. Mater. Sci.*, 1994, **29**, 4351–4356.
7. Li, P. and Chen, I. W., Effect of dopants on zirconia stabilization-an X-ray absorption study: II, tetravalent dopants. *J. Am. Ceram. Soc.*, 1994, **77**(5), 1281–1288.
8. Maschio, S., Sbaizero, O., Meriani, S. and Bischoff, E., Sintering aids for ceria-zirconia alloys. *J. Mater Sci.*, 1992, **27**, 2734–2738.
9. Reidy, R. F. and Simkovich, G., Electrical conductivity and point defect behavior in ceria-stabilized zirconia. *Solid State Ion.*, 1993, **62**, 85–97.
10. Steele, B. C. H., In *High Conductivity Solid Ionic Conductors, Recent Trends and Applications*, ed. T. Takahashi. World Scientific, Singapore, 1989, pp. 402–446.
11. Badwal, S. P. S., In *Materials Science and Technology, A Comprehensive Treatment*. ed. R. W. Cahn, P. Haasen and E. J. Kramer, Vol 11. VCH, Weinheim, Germany, 1994, p. 567.
12. Badwal, S. P. S., Drennan, J., Hughes, A. E., In: *Science of Ceramic Interfaces*, ed. J. Nowotny. Elsevier, Amsterdam, 1991, pp. 227–284.
13. Gerhardt, R. and Nowick, A. S., Grain-boundary effect in ceria doped with trivalent cations: I, electrical measurements. *J. Am. Ceram. Soc.*, 1986, **69**(9), 641–646.
14. Verkerk, M. J., Middlehuis, B. J. and Burggraaf, A. J., *Solid State Ion.*, 1982, **6**, 159.
15. Kleitz, M., Bernard, H., Fernandez, E. and Schouler, E., In *Science and Technology of Zirconia, Advances in Ceramics*, Vol 3, ed. A. H. Heuer and L. W. Hobbs. The Am. Ceram. Soc. Columbus, OH, 1981 pp. 310–336.

16. Kobayashi, S., X-ray microanalysis of the boundary phase in partially stabilized zirconia (PSZ). *J. Mater. Sci. Lett.*, 1985, **4**(3), 268–270.
17. Narasimha Rao, B. V. and Schreiber, T. P., Scanning transmission electron microscope analysis of solute partitioning in a partially stabilized zirconia. *J. Am. Ceram. Soc.*, 1982, **65**(3), C44–C45.
18. Chaim, R., Brandon, D. G. and Heuer, A. H., A Diffusional phase transformation in ZrO_2-4 wt% Y_2O_3 induced by surface segregation. *Acta Metal.*, 1986, **34**(10), 1933–1939.
19. Theunissen, G. S. A. M., Winnubst, A. J. A. and Burggraaf, A. J., Segregation aspects in the ZrO_2–Y_2O_3 ceramics system. *J. Mater. Sci. Lett.*, 1989, **8**(1), 55–57.
20. Hughes, A. E. and Badwal, S. P. S., Impurity and yttrium segragation in yttria-tetragonal zirconia. *Solid State Ion.*, 1991, **46**(3–4), 265–274.
21. Badwal, S. P. S., Electrical conductivity of single crystal and polycrystalline ytria-stabilized zirconia. *J. Mater. Sci.*, 1984, **19**, 1767–1976.